



# A novel design of high performance all-optical encoder using PhCRR

Ehsan Veisi<sup>1</sup> · Mahmood Seifouri<sup>1</sup> · Saeed Olyae<sup>2</sup> 

Received: 6 February 2022 / Accepted: 20 April 2022 / Published online: 20 May 2022

© The Author(s), under exclusive licence to Springer Science+Business Media, LLC, part of Springer Nature 2022

## Abstract

This study aims to use a new approach to construct and simulate an innovative nanostructure for an all-optical encoder (AOE) employing a ring resonator. In encryption systems, encoders are utilized. The plane wave expansion (PWE) approach was used to examine the frequency modes as well as encoder design. Apart from optimizations, the suggested design was numerically analyzed and simulated utilizing the finite-difference time-domain (FDTD) numerical solution technique. The radius of the rods, the core rods' radius, and the nanostructure's wavelength were adjusted to create the desired nanostructure. The suggested AOE uses an ultra-compact nanostructure with a footprint of  $108 \mu\text{m}^2$ . The suggested nanostructure's outstanding contrast ratio (16.4 dB) was one of its distinctive properties compared to other nanostructures. This nanostructure had a delay time of 530 fs and a bit rate of 1.88 Tb/s. The simulations have been conducted at a central wavelength of  $1.55 \mu\text{m}$ , demonstrating that the suggested nanostructure is appropriate for usage in the third telecommunication window. A photonic crystal ring resonator (PhCRR) that may be employed in integrated optical circuits has been utilized to design the high-efficiency encoder.

**Keywords** Photonic crystal ring resonator (PhCRR) · All-optical encoder (AOE) · Nonlinear Kerr effect · Optimization

## 1 Introduction

Photonic crystals with a variable refractive index could be utilized to regulate and direct light output if the periodic pattern is replicated in two dimensions, the two-dimensional photonic crystal structure (Yablonovitch 1987; John 1987; Yablonovitch et al. 1991; Sibilia et al. 2008). Due to the significant resemblance between the Schrödinger equation in solid-state physics as well as the Helmholtz equation in the setting of the electric field, photonic crystal formations could be referred to as dual

---

✉ Saeed Olyae  
s\_olyae@sru.ac.ir

<sup>1</sup> Faculty of Electrical Engineering, Shahid Rajaee Teacher Training University, Tehran, Iran

<sup>2</sup> Nano-Photonics and Optoelectronics Research Laboratory (NORLab), Shahid Rajaee Teacher Training University, Tehran 16788-15811, Iran

semiconductor crystals (Quimby 2006). For instance, in the Schrödinger equation, the electric potential is analogous to the refractive index in the Helmholtz equation (Baba 2008; Saha and Sen 2020). As a result, photonic crystals have a nearly identical functionality against photons as semiconductor crystals perform against electrons (Baba 2008; Saha and Sen 2020). All-optical photonic crystal devices are expanding and evolving (Mohammadi et al. 2019, 2022; He et al. 2020; Serajmohammadi et al. 2019; Rajasekar et al. 2019; Mohammadi and Seifouri 2019; Moradi et al. 2021; Foroughifar et al. 2021; Cheshmberah et al. 2021). Encoders and decoders are integral components of optical signal processing systems, all-optical networks, as well as all optical processors, contributing tremendously to their effectiveness (Xavier et al. 2016; Younis et al. 2014; D'souza and Mathew 2016). The study of photonic crystal digital devices, such as logic gates (Mohebzadeh-Bahabady and Olyaei 2018; He et al. 2019; Ge et al. 2020; Veisi et al. 2021) and analog-to-digital converters (Mehdizadeh et al. 2017; Geng and Zhao 2020), is becoming a substantial area of research for the scientific world. Lately, considerable research on the design of encoders has been undertaken (Lee et al. 2009; Hassangholizadeh-Kashtiban et al. 2015; Moniem 2016; Seif-Dargahi 2018; Parandin 2019; Monisha et al. 2019; Naghizade and Saghaei 2020; Rajasekar et al. 2020, 2021; Mohebzadeh-Bahabady and Olyaei 2020; Fallahi et al. 2021; Hamedi et al. 2021). For an encoder with a  $598 \mu\text{m}^2$  footprint, Hassangholizadeh et al. have suggested a Kerr effect-based structure; however, there is no information regarding their suggested structure's time response or contrast ratio (Hassangholizadeh-Kashtiban et al. 2015).

Seif-Dargahi generated a two-dimensional photonic crystal structure for an encoder and examined it at a wavelength of  $1,555 \mu\text{m}$ , and displayed a contrast ratio of 9.2 dB and time response of 1.8 ps, respectively (Seif-Dargahi 2018). The designed structure's downside was its extraordinarily huge size. Monisha et al. also created a mechanism for an encoder with an 8 dB contrast ratio; however, there is no information about the structure's time response or footprint (Monisha et al. 2019). Rajasekar et al. developed an innovative Barium Titanate rods-based structure in the airbed for a  $\sim 174 \mu\text{m}$  encoder with a contrast ratio of 7.11 dB (Rajasekar et al. 2020). Mohebzadeh and Olyaei have presented a novel all-optical encoder with a contrast ratio of 9.51 dB depending on silicon dielectric rods in air (Mohebzadeh-Bahabady and Olyaei 2020). Fallahi et al. utilized scattering rods and nano-resonators to create an optimized and asymmetric encoder with a contrast ratio of 7.8 dB regardless of relatively low reaction time (Fallahi et al. 2021). The interference mechanism was employed in the light diffusion in the encoder structure, and silicon rods were utilized in the airbed to construct a symmetric encoder. Recently, Rajasekar et al. devised a high-speed encoder relying on  $\text{BaTiO}_3$  in the air having a time delay of  $\sim 375$  s, a bit rate of 2.66 Tb, as well as a contrast ratio of 10.4 dB (Rajasekar et al. 2021). Furthermore, because of its high efficacy,  $\text{BaTiO}_3$  is typically employed in nonlinear modes; however, in this study, only the linear function of the material was regarded for the encoder (Quimby 2006).

A PhCRR-based encoder was suggested in this research, and its efficiency was assessed utilizing the FDTD numerical solution technique, yielding a footprint of  $108 \mu\text{m}^2$ , a delay time of  $\sim 530$  fs, and a bit rate of 1.88 Tb/s. The suggested encoder structure has the distinct benefit of distinguishing logic 0 from logic one due to its outstanding contrast ratio. In the linear model, the contrast ratio of the suggested encoder nanostructure is approximately 16.4 dB, which is the highest contrast ratio among other systems described.

## 2 AOE nanostructure design

### 2.1 Binary encoder $2^N$ to N

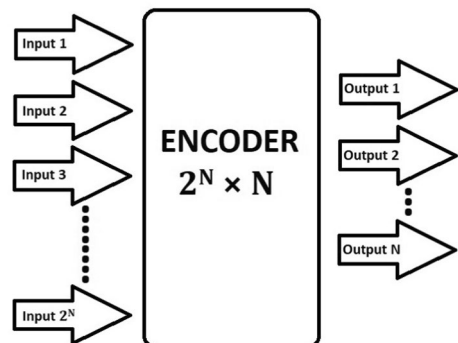
Encoders are employed in a variety of systems for encryption.  $2^N$  bits are converted to N bits via an N-bit encoder in the output. For instance, whether an encoder has three bits, eight input modes, and three output modes must be regarded. Encoders can be categorized into two classes: Priority encoders and Binary encoders (Mano 2002; Brown 2010; Holdsworth and Woods 2002). Binary encoder is mentioned in the paper (Mano 2002; Brown 2010; Holdsworth and Woods 2002). In the priority encoder, if another input is on, encryption will be performed based on the priority of the inputs. A  $4 \times 2$  binary encoder that is the number of bits required to encode two bits, would be used in this work by having four input modes as well as two output modes. If the input values are "1000," the coded output value is "00," if the input values are equivalent to "0100," the coded output value is "01," and if the input values are comparable to "0010," the output values are "10." In the other scenario, where the input value is equal to "0001," the output values are identical to "11," and therefore, the information is presented as encoded in the binary encoder output. The encoder is shown in Fig. 1.

### 2.2 Calculation of photonic band gaps and AOE nanostructure optimization

A  $21 \times 19$  two-dimensional photonic crystal structure containing Si rods in air with triangular lattice is used to design the AOE. Figure 2 shows the first Brillouin zone for the proposed nanostructure next to the TM band structure. As shown in Fig. 2, the proposed structure has two band gaps for TM mode. We used the first band gap of the structure to design the proposed AOE. The range of the first band gap includes frequencies from  $a/\lambda = 0.269$  to  $a/\lambda = 0.430$ . The encoder is designed with four waveguides for the input light sources, a PhCRR, and two waveguides for measuring the light output power. The lattice constant of the nanostructure is 556 nm, the radius of the Si rods after optimizing the structure is equal to 117 nm. The wavelength range in the first band gap is between 1293 and 2066 nm.

The optimum central wavelength of 1.55  $\mu\text{m}$  is obtained for the nanostructure that the suggested nanostructure is appropriate for usage in the third telecommunication window and the radius of the PhCRR core rods after AOE optimization is 113 nm. Of course, in designing the structure, it has been taken into account that if the radius of  $\pm 1$  nm of each of

Fig. 1 Encoder scheme



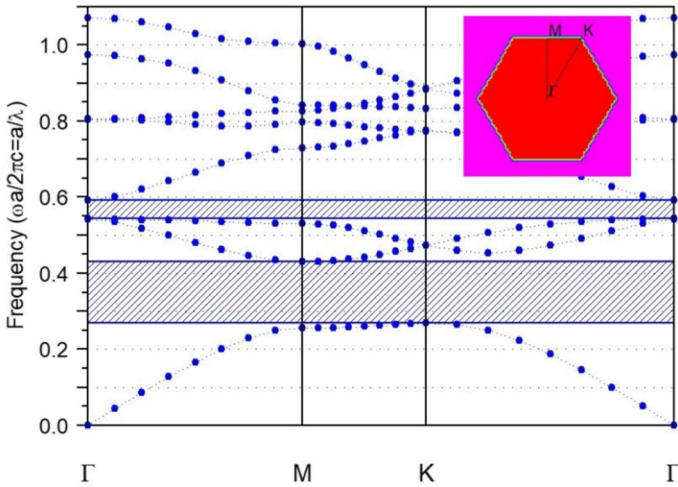


Fig. 2 TM band structure and the first Brillouin zone

the rods is changed, the AOE performance will not decrease much. The proposed encoder structure is shown in Fig. 3.

The aim of designing an optimum structure for an all-optical encoder is to accomplish an ultra-compact structure, which in addition to reducing the size of the structure, escalating the effectiveness of the structure and escalating the bit rate is also significant. To optimize the radius of the AOE core rods, we examined the outputs of the structure while the fourth input is on. As can be seen in Fig. 4, in the radii of 112 nm to 114 nm, the output values will be optimal in the fourth case. If the core rod radius is shorter than the current state, the resonator will provide a weaker transmission rate performance. Also if the core rod radius is longer than the

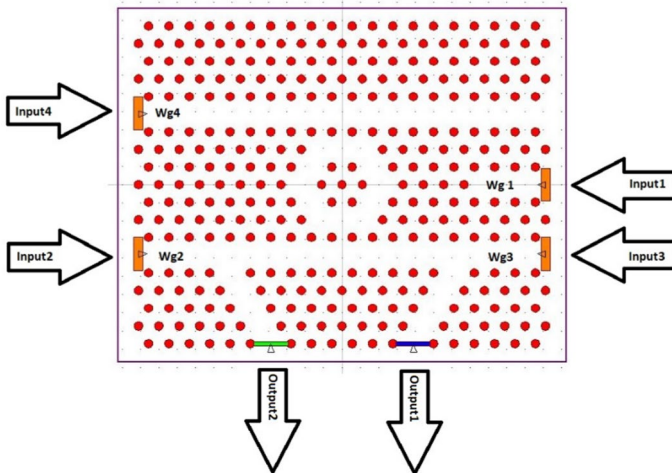
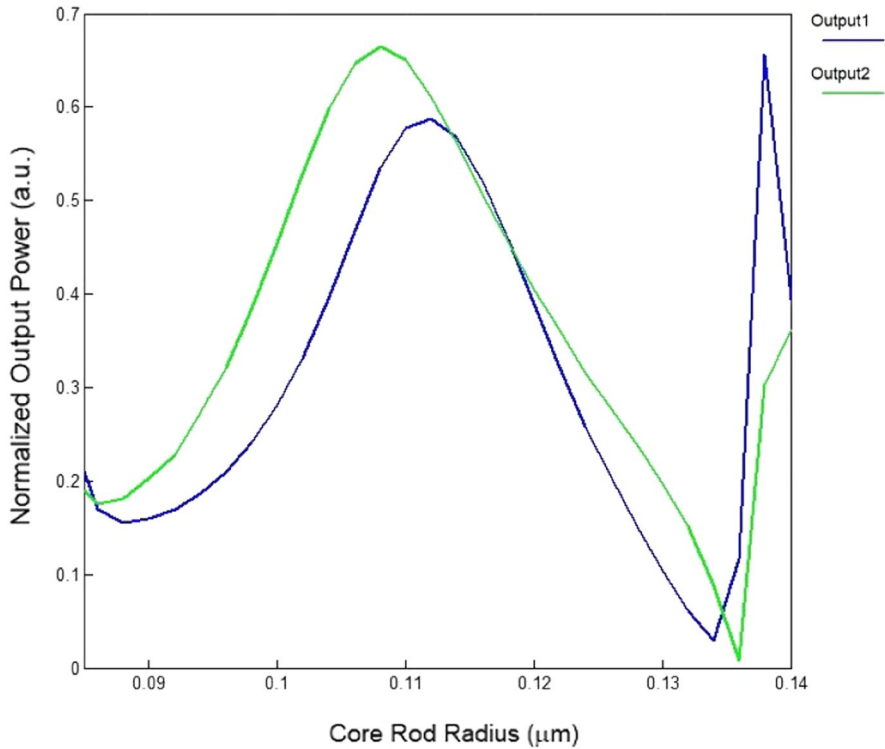


Fig. 3 The proposed AOE



**Fig. 4** AOE core rod radius optimization

current state, the resonator will provide a weaker transmission rate performance. In this case, the optimal radius of the core rod for us will be where the two outputs have the highest amount of transmission. The reason for choosing a radius of 113 nm is the  $\pm 1$  nm tolerance of the radius of these rods, which may occur in the fabrication for the radius of the rods. The radius of the AOE core rods from 90 to 125 nm will not disturb the performance of the encoder, but if the radius of these rods exceeds 125 nm, the structure will intensify and the encoder performance will be disturbed.

The rods radius of the AOE for both outputs of the structure is given in Fig. 5 as the highest value of state zero and the lowest value of state one. The output for radii of 116 nm to 118 nm in the ON state will be about 0.35. Also, the output for radii of 117 to 118 nm in the off state will be equal to about 0.007. Based on this, a radius of 117 nm has been selected for Si rods. The optimal mode selection is when there is the largest difference between zero and one mode. In this case, the AOE performance will be the most optimal mode possible. Figure 5 shows these values for radii of 115 nm to 125 nm in ON and OFF mode.

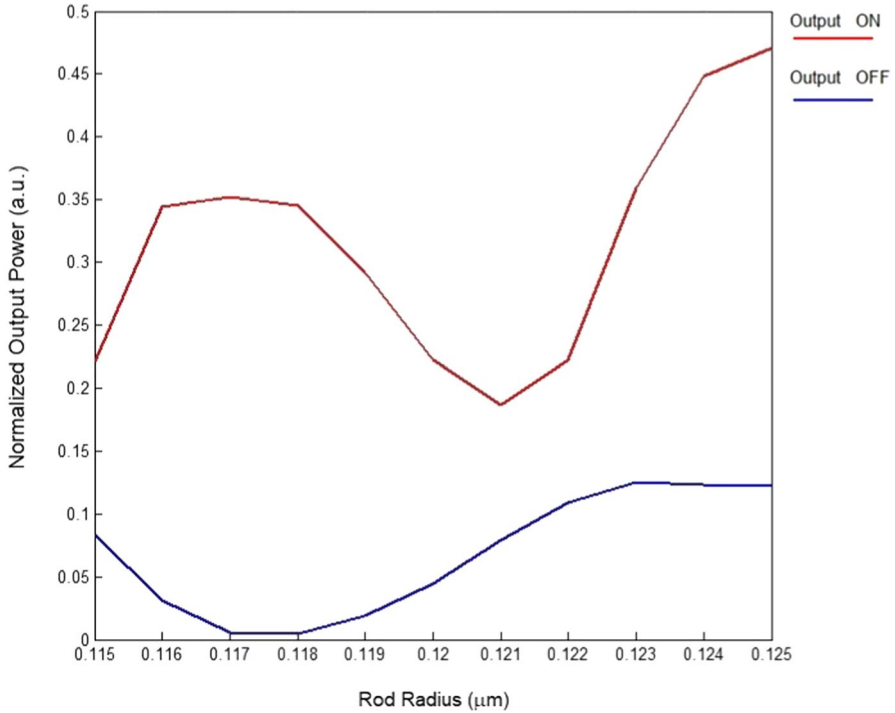


Fig. 5 AOE rod radius optimization

### 3 Numerical analysis of the proposed AOE nanostructure

The nanostructure of the encoder will be simulated and numerically analyzed. The FDTD approach was employed in the numerical analysis of the suggested encoder nanostructure. The normalized Maxwell equations are presented in Eqs. (1)–(3) for FDTD numerical analysis (Veisi et al. 2022; Houle and Sullivan 2020):

$$\frac{\partial \tilde{D}}{\partial t} = \frac{1}{\sqrt{\epsilon_0 \mu_0}} \nabla \times H \tag{1}$$

$$\tilde{D}(\omega) = \epsilon_r^*(\omega) \cdot \tilde{E}(\omega) \tag{2}$$

$$\frac{\partial H}{\partial t} = -\frac{1}{\sqrt{\epsilon_0 \mu_0}} \nabla \times \tilde{E} \tag{3}$$

The utilization of TM mode in Ez, Hx, and Hz nanostructure is considered for the preceding equations. By substituting Ez, Hx, and Hz into the preceding equation, we obtain (Veisi et al. 2022; Houle and Sullivan 2020):

$$\frac{\partial D_z}{\partial t} = \frac{1}{\sqrt{\epsilon_0 \mu_0}} \left( \frac{\partial H_y}{\partial t} - \frac{\partial H_x}{\partial t} \right) \tag{4}$$

$$D_z(\omega) = \epsilon_r^*(\omega) \cdot E_z(\omega) \tag{5}$$

$$\frac{\partial H_x}{\partial t} = -\frac{1}{\sqrt{\epsilon_0 \mu_0}} \frac{\partial E_z}{\partial y} \tag{6}$$

$$\frac{\partial H_y}{\partial t} = \frac{1}{\sqrt{\epsilon_0 \mu_0}} \frac{\partial E_z}{\partial x} \tag{7}$$

where,  $\epsilon_0$  and  $\mu_0$  are the permittivity of free space and the permeability of free space, respectively. The perfectly matched layers (PML) is one of the most adaptable and successful attracting ABCs in boundary conditions. The return value of the wave is determined from the equation as it propagates from medium A ( $\eta_A$ ) to medium B ( $\eta_B$ ) (Veisi et al. 2022; Houle and Sullivan 2020):

$$\Gamma = \frac{\eta_A - \eta_B}{\eta_A + \eta_B} \tag{8}$$

The impedances of media A and B are determined from the underlying equation. The best ideal scenario in Eq. (8) is for media A's impedance to be near media B's. This means that the return wave will be close to Zero. The impedance of the media is obtained from Veisi et al. (2022):

$$\eta = \sqrt{\frac{\mu}{\epsilon}} \tag{9}$$

where,  $\epsilon$  and  $\mu$  are the permittivity and the permeability, respectively. These values are obtained from:

$$\epsilon = \epsilon_0 \times \epsilon_r \tag{10}$$

$$\mu = \mu_0 \times \mu_r \tag{11}$$

In this research, the meshing approach is as follows:  $\Delta y$  and  $\Delta x$  are the minimal size values for meshing in the y and x directions, respectively, equal to  $\lambda / 16$ . In this situation,  $\Delta t$  values will be determined utilizing Eq. (12):

$$\Delta t < \frac{1}{c \sqrt{\left(\frac{1}{\Delta x}\right)^2 - \left(\frac{1}{\Delta y}\right)^2}} \tag{12}$$

### 3.1 Case1

In the first case, which we will examine for encoder, the light source will be ON. The final value of two outputs one and two in this case is less than 0.0001 the amount of

input light power. In this case, the two outputs are equal to logic zero and will encode “1000” to “00”. The field distribution and time response diagram in this case is shown in Fig. 6.

### 3.2 Case2

In the second case, which was analyzed, the input light source 2 is on and the other light sources are off. The field distribution diagram and frequency response of this case are shown in Fig. 7. The value of the first output is equal to 0.008 of the input light power and the value of the second output is equal to 0.35 of the input light power. The second output in this case will be equal to the logical ON and the first output will be in the OFF mode. The amount of time delay in this case is about 238 femtoseconds.

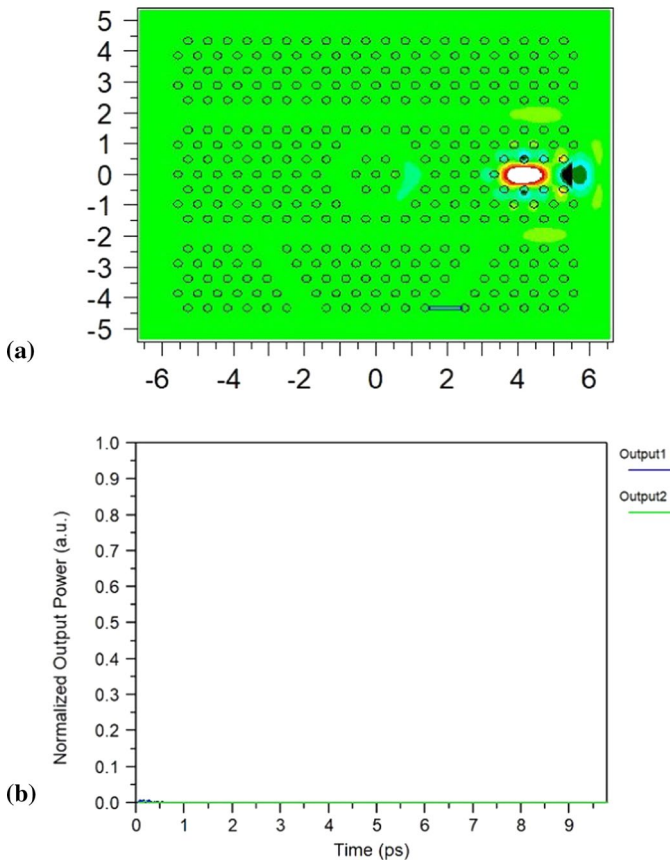


**Fig. 6** **a** Case 1 in which input port input1 is On, and another inputs are Off. The outputs become Off ( $<0.0001 \text{ W}/\mu\text{m}^2$ ). **b** Response time of case 1



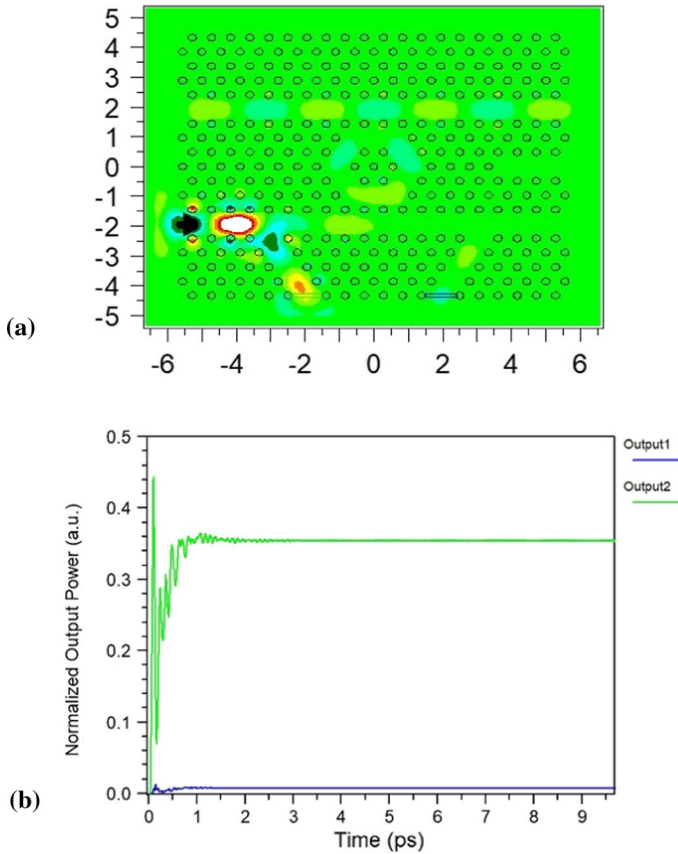


**Fig. 7** **a** Case 2 in which input port input2 is On, and another inputs are Off. The output1 becomes Off ( $0.008 \text{ W}/\mu\text{m}^2$ ), and the output2 becomes Off ( $0.35 \text{ W}/\mu\text{m}^2$ ). **b** Response time of case 2

### 3.3 Case3

In the third case, due to the relative symmetry in the proposed encoder structure, the conditions will be inverse of the second case. In this case, the third input will be on. The value of the first output in this case will be equal to 0.35 of the input light power and equal to one logic. The value of the second output in this case will be equal to 0.008 of the input light power and equal to zero logic. The amount of time delay in this case will be the same as in the second case. The encrypted value in this case will be equal to “10”. The field distribution diagram and frequency response of this case are shown in Fig. 8.

### 3.4 Case 4

In the fourth case, the fourth input light source will be on. In this case, the two proposed encoder outputs must be equal to one logic. As can be seen in Fig. 9, in the fourth case

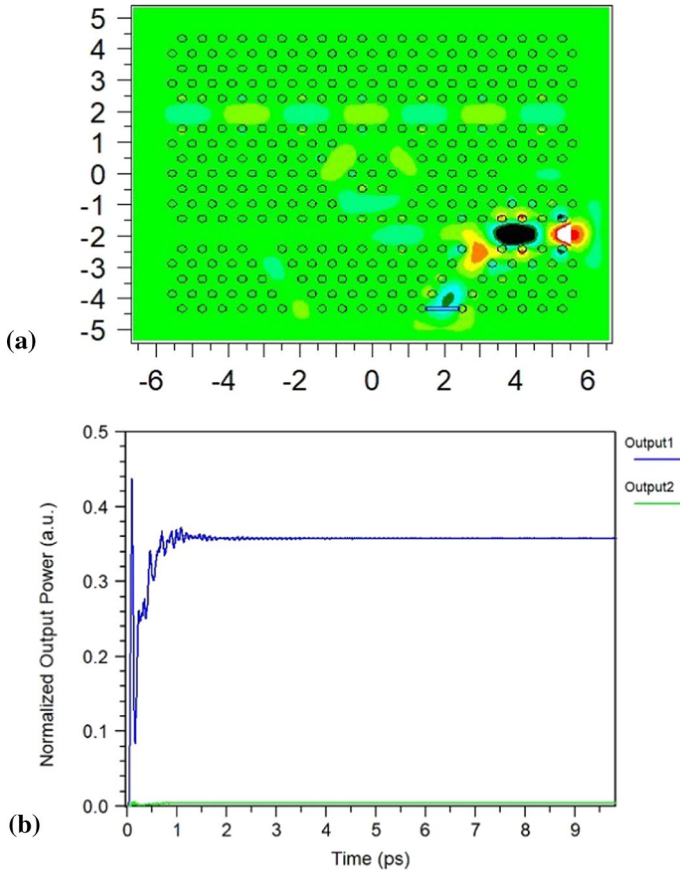


**Fig. 8** **a** Case 2 in which input port input3 is On, and another inputs are Off. The output1 becomes On ( $0.35 \text{ W}/\mu\text{m}^2$ ), and the output2 becomes Off ( $0.008 \text{ W}/\mu\text{m}^2$ ). **b** Response time of case 3

the two outputs are equal and in the on position. In this case, the time delay is about 530 femtoseconds. The bit rate will be 1.88 Tb/s. The normalized output value for the two output ports will be  $0.58 \text{ W}/\mu\text{m}^2$ , as shown in Fig. 9 and the encrypted value will be equal to “11”. Detailed analysis will follow in the following sections.

### 3.5 Nonlinear case

All the analyzes examined in the previous section were in linear mode. The structure exhibited at low power intensities does not rely on the power intensity, but in the nonlinear state, with enhancing the intensity of input power, unwanted conditions might happen for the structure, which were studied by inspecting the structure in the nonlinear state. In this section, we want to analyze all of the above by applying a nonlinear Kerr effect. In the nonlinear case, the refractive index will be obtained from the following equation (Veisi et al. 2021).

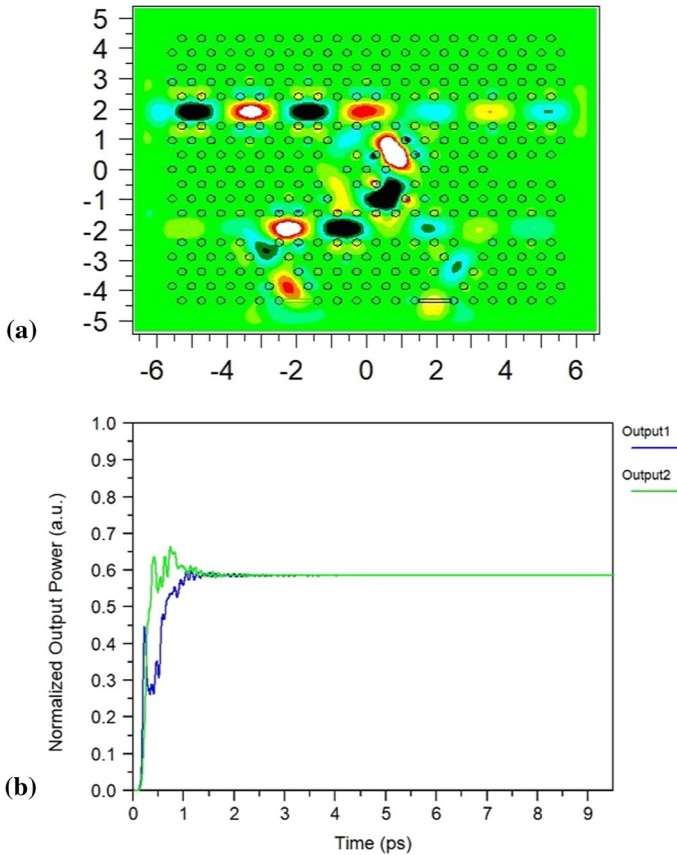


**Fig. 9** **a** Case 4 in which input port input4 is On, and another inputs are Off. The outputs become ON (less than  $0.58 \text{ W}/\mu\text{m}^2$ ). **b** Response time of case 4

$$n = n_0 + n_2 I \tag{13}$$

where,  $I$  is the intensity,  $n_2$  is the nonlinear refractive index and  $n_0$  is the free space refractive index and depends on the wavelength (Veisi et al. 2021). The nonlinear refractive index of silicon is equal to  $1.5 \times 10^{-17} \text{ m}^2/\text{W}$  and the amount of light intensity in this case is equal to  $100 \text{ W}/\mu\text{m}^2$  (Veisi et al. 2021). The values obtained in the four cases examined are given in Table 1.

## 4 Discussion and compare of the all-optical $4 \times 2$ encoder performance

### 4.1 Evaluation based on contrast ratio

The contrast ratio is presented in this section to assess the suggested encoder’s performance. The contrast ratio is the differential in values between the ON as well as OFF states

**Table 1** Nonlinear case values

Case	Nonlinear encoder input values				Nonlinear encoder outputs values	
	Input1(W/ $\mu\text{m}^2$ )	Input2(W/ $\mu\text{m}^2$ )	Input3(W/ $\mu\text{m}^2$ )	Input4(W/ $\mu\text{m}^2$ )	Output1(W/ $\mu\text{m}^2$ )	Output2(W/ $\mu\text{m}^2$ )
1	100 (ON)	0 (OFF)	0 (OFF)	0 (OFF)	0.2 (OFF)	0.2 (OFF)
2	0 (OFF)	100 (ON)	0 (OFF)	0 (OFF)	3.3 (OFF)	34 (ON)
3	0 (OFF)	0 (OFF)	100 (ON)	0 (OFF)	34 (ON)	3.3 (OFF)
4	0 (OFF)	0 (OFF)	0 (OFF)	100 (ON)	68 (ON)	53 (ON)

of output, and The high contrast ratio demonstrates the encoder’s appropriate functioning. Equation specifies the contrast ratio (CR) (Veisi et al. 2021):

$$CR(dB) = 10\log \frac{Output(i)_{ON}}{Output(i)_{OFF}} \tag{14}$$

The values obtained for the linear mode and the CR are given in Table 2.

### 4.2 Evaluate the performance of the proposed all-optical 4 × 2 encoder

In the previous section, the output values for the structure were analyzed and evaluated. In this section, we will review and analyze the proposed AOE in comparison with other proposed all-optical encoders. The contrast ratio will be 16.4 dB in the linear mode and 10.12 dB in the nonlinear mode. As you can see in Table 3, the performance of the proposed nanostructure compared to other structures presented will be very good and optimal in both linear and nonlinear modes.

## 5 Conclusion

This research discusses the design, simulation, and evaluation of an ultra-compact as well as ultra-fast encoder nanostructure. The encoder suggested here is optimized for rod radius, core rod radius, and wavelength of the input light source. The PWE approach was utilized for designing the suggested encoder, and the FDTD method was employed to get

**Table 2** The proposed AOE performance

Case	Encoder input values				Encoder outputs values	
	Input1	Input2	Input3	Input4	Output1	Output2
1	Pin	0	0	0	0.0001Pin(OFF)	0.0001Pin(ON)
2	0	Pin	0	0	0.008Pin(OFF)	0.35Pin(ON)
3	0	0	Pin	0	0.35Pin(ON)	0.008Pin(OFF)
4	0	0	0	Pin	0.58Pin(ON)	0.58Pin(ON)
	Contrast ratio(dB)				16.4 dB	16.4 dB

**Table 3** Compare the proposed all-optical 4×2 encoder with similar works

References	Mechanism	Material	Footprint ( $\mu\text{m}^2$ )	CR(dB)
Hassangholizadeh-Kashtiban et al. (2015)	Nonlinear	Si in air	598	–
Monisha et al. (2019)	Linear	Si in air	196	16.5
Parandin (2019)	Linear	Si in air	–	8
Seif-Dargahi (2018)	Linear	Si in air	880	9.2
Fallahi et al. (2021)	Linear	Si in air	149	7.88
Rajasekar et al(2021)	Linear	LiBO3 in air	179	10.4
Rajasekar et al(2020)	Linear	LiBO3 in air	174	7.11
This work	Nonlinear	Si in air	108	10.13
This work	Linear	Si in air	108	16.4

numerical outcomes and simulate the recommended nanostructure. The suggested ultra-compact nanostructure footprint is approximately  $108 \mu\text{m}^2$ , with a nanostructure delay time of roughly 530 fs. Another aspect discussed in this study is the encoder's superior contrast ratio in comparison to other encoders. The suggested encoder's high bit rate seems to be another distinguishing characteristic. The bit rate is obtained 1.88 Tb/s. The suggested encoder may be employed in all-optical integrated circuits with distinct properties.

**Acknowledgements** This work has been done in Nano-photonics and Optoelectronics Research Laboratory (NORLab), Shahid Rajae University.

**Authors' contributions** EV: data curation, writing—original draft, MS and SO: supervision, writing – review and editing. All authors read and approved the final manuscript.

**Funding** The authors have not disclosed any funding.

## Declarations

**Conflict of interest** The authors declare that they have no known competing financial interests or personal relationships that could have appeared to influence the work reported in this paper.

**Consent to participate** Yes.

**Consent for publication** The authors gave consent for publication as per the journal standard.

**Ethics approval** The authors declared that the manuscript ethics is approved as per the journal.

## References

- Baba, T.: Slow light in photonic crystals. *Nat. Photonics* **2**(8), 465–473 (2008)
- Brown, S.: *Fundamentals of Digital Logic Design with VHDL*. Mc Graw Hill, Higher Education (2010)
- Cheshmberah, A., Seifouri, M., Olyae, S.: Design of all-normal dispersion with Ge11. 5As24Se64. 5/Ge20Sb15Se65 chalcogenide PCF pumped at 1300 nm for supercontinuum generation. *Opt. Quant. Electron.* **53**(8), 1–11 (2021)
- D'souza, N.M., Mathew, V.: Interference based square lattice photonic crystal logic gates working with different wavelengths. *Opt. Laser Technol.* **80**, 214–219 (2016)

- Fallahi, V., Mohammadi, M., Kordrostami, Z., Seifouri, M., Olyae, S.: Design and optimization of an ultra-fast symmetrical  $4 \times 2$  encoder based on 2D photonic crystal nano-resonators for integrated optical circuits. *Opt. Quant. Electron.* **53**(10), 1–18 (2021)
- Foroughifar, A., Saghaei, H., Veisi, E.: Design and analysis of a novel four-channel optical filter using ring resonators and line defects in photonic crystal micronanostructure. *Opt. Quant. Electron.* **53**(2), 1–12 (2021)
- Ge, R., Yan, B., Xie, J., Liu, E., Tan, W., Liu, J.: Logic gates based on edge states in gyromagnetic photonic crystal. *J. Magn. Magn. Mater.* **500**, 166367 (2020)
- Geng, X., Zhao, L.: All-optical analog to digital converter based on nonlinear photonic crystal ring resonators. *Photonics Nanostructures-Fundam. Appl.* **41**, 100817 (2020)
- Hamed, S., Negahdari, R., Ansari, H. R.: Design plasmonic optical  $4 \times 2$  encoder based on 2D photonic crystal ring resonator. *Plasmonics*, pp. 1–8, (2021)
- Hassangholizadeh-Kashitban, M., Sabbaghi-Nadooshan, R., Alipour-Banaei, H.: A novel all optical reversible  $4 \times 2$  encoder based on photonic crystals. *Optik* **126**(20), 2368–2372 (2015)
- He, L., Ji, H., Wang, Y., Zhang, X.: Topologically protected beam splitters and logic gates based on two-dimensional silicon photonic crystal slabs. *Opt. Express* **28**(23), 34015–34023 (2020)
- He, L., Zhang, W., Zhang, X.: Topological all-optical logic gates based on two-dimensional photonic crystals. *Opt. Express* **27**(18), 25841–25859 (2019)
- Holdsworth, B., Woods, C.: *Digital Logic Design*. Elsevier, Amsterdam (2002)
- Houle, J.E., Sullivan, D.M.: *Electromagnetic Simulation Using the FDTD Method with Python*. John Wiley and Sons, New Jersey (2020)
- John, S.: Strong localization of photons in certain disordered dielectric superlattices. *Phys. Rev. Lett.* **58**(23), 2486–2490 (1987)
- Lee, K.-Y., Yang, Y.-C., Lin, Y.-J., Lee, W.-Y., Lee, C.-C., Wong, S.-H.: The designs of  $4 \times 2$  encoder based on photonic crystals. Asia Communications and Photonics conference and Exhibition (ACP) (2009)
- Mano, M. M.: *Digital design*. Pearson Educación, (2002)
- Mehdizadeh, F., Soroosh, M., Alipour-Banaei, H., Farshidi, E.: A novel proposal for all optical analog-to-digital converter based on photonic crystal nanostructures. *IEEE Photonics J.* **9**(2), 1–11 (2017)
- Mohammadi, M., Olyae, S., Seifouri, M.: Passive integrated optical gyroscope based on photonic crystal ring resonator for angular velocity sensing. *SILICON* **11**(6), 2531–2538 (2019)
- Mohammadi, M., Seifouri, M.: Numerical investigation of photonic crystal ring resonators coupled bus waveguide as a highly sensitive platform. *Photonics Nanostructures-Fundam. Appl.* **34**, 11–18 (2019)
- Mohammadi, M., Farahmand, M., Olyae, S., Seifouri, M.: An overview of all-optical memories based on periodic structures used in integrated optical circuits. *Silicon*, pp. 1–20 (2022)
- Mohebzadeh-Bahabady, A., Olyae, S.: All-optical NOT and XOR logic gates using photonic crystal nano-resonator and based on an interference effect. *IET Optoelectron.* **12**(4), 191–195 (2018)
- Mohebzadeh-Bahabady, A., Olyae, S.: Designing an ultracompact all-optical 4-to-2 encoder and investigating its optical power consumption. *Appl. Opt.* **59**(8), 2409–2415 (2020)
- Moniem, T.A.: All-optical digital  $4 \times 2$  encoder based on 2D photonic crystal ring resonators. *J. Mod. Opt.* **63**(8), 735–741 (2016)
- Monisha, S., Saranya, D., Rajesh, A.: Design and analysis of multi-hexagonal reversible encoder using photonic crystals. *Opt. Quant. Electron.* **51**(1), 1–12 (2019)
- Moradi, M., Mohammadi, M., Olyae, S., Seifouri, M.: Design and simulation of a fast all-optical modulator based on photonic crystal using ring resonators. *SILICON* **13**(1), 1–7 (2021)
- Naghizade, S., Saghaei, H.: A novel design of all-optical 4 to 2 encoder with multiple defects in silica-based photonic crystal fiber. *Optik* **222**, 165419 (2020)
- Parandin, F.: High contrast ratio all-optical  $4 \times 2$  encoder based on two-dimensional photonic crystals. *Opt. Laser Technol.* **113**, 447–452 (2019)
- Quimby, R.S.: *Photonics and Lasers*. John Wiley and Sons Inc, New Jersey (2006)
- Rajasekar, R., Jayabarathan, J.K., Robinson, S.: Nano-optical filter based on multicavity coupled photonic crystal ring resonator. *Phys. E Low-Dimensional Syst. Nanostruct.* **114**, 113591 (2019)
- Rajasekar, R., Raja, G.T., Jayabarathan, J.K., Robinson, S.: High speed nano-optical encoder using photonic crystal ring resonator. *Photon Netw. Commun.* **40**(1), 31–39 (2020)
- Rajasekar, R., Raja, G.T., Robinson, S.: Numerical analysis of reconfigurable and multifunctional barium titanate platform based on photonic crystal ring resonator. *IEEE Trans. Nanotechnol.* **20**, 282–291 (2021)
- Saha, P., Sen, M.: NOEMS Based Slotted Photonic Crystal Cavity for the Sensing of Force. *IEEE Trans. Nanotechnol.* **20**, 20–27 (2020)
- Seif-Dargahi, H.: Ultra-fast all-optical encoder using photonic crystal-based ring resonators. *Photon Netw. Commun.* **36**(2), 272–277 (2018)

- Serajmohammadi, S., Alipour-Banaei, H., Mehdizadeh, F.: A novel proposal for all optical 1-bit comparator using nonlinear PhCRRs. *Photonics Nanostructures-Fundam. Appl.* **34**, 19–23 (2019)
- Sibilia, C., Benson, T.M., Marciniak, M., Szoplik, T.: *Photonic Crystals: Physics and Technology*. Springer, Berlin (2008)
- Veisi, E., Seifouri, M., Olyae, S.: A novel design of all-optical high speed and ultra-compact photonic crystal and logic gate based on the Kerr effect. *Appl. Phys. B* **127**(5), 1–9 (2021)
- Veisi, E., Seifouri, M., Olyae, S.: Design and numerical analysis of multifunctional photonic crystal logic gates. *Opt. Laser Technol.* **151**, 108068 (2022)
- Xavier, S.C., Carolin, B.E., Kabilan, A.P., Johnson, W.: Compact photonic crystal integrated circuit for all-optical logic operation. *IET Optoelectron.* **10**(4), 142–147 (2016)
- Yablonovitch, E.: Inhibited spontaneous emission in solid-state physics and electronics. *Phys. Rev. Lett.* **58**(20), 2059–2064 (1987)
- Yablonovitch, E., Gmitter, T., Leung, K.-M.: Photonic band nanostructure: The face-centered-cubic case employing nonspherical atoms. *Phys. Rev. Lett.* **67**(17), 2295–2299 (1991)
- Younis, R.M., Areed, N.F., Obayya, S.S.: Fully integrated AND and OR optical logic gates. *IEEE Photonics Technol. Lett.* **26**(19), 1900–1903 (2014)

**Publisher's Note** Springer Nature remains neutral with regard to jurisdictional claims in published maps and institutional affiliations.